Check for updates

How to cite: *Angew. Chem. Int. Ed.* **2024**, *63*, e202408335
doi.org/10.1002/anie.202408335

Gold Clusters | Hot Paper

Gas-Phase Anion Photoelectron Spectroscopy of Alkanethiolate-Protected $PtAu_{12}$ Superatoms: Charging Energy in Vacuum vs Solution

Yuriko Tasaka, Megumi Suyama, Shun Ito, Kiichirou Koyasu, Manfred Kappes, Flavio Maran,* and Tatsuya Tsukuda**

Abstract: The charging behavior of molecular Au clusters protected by alkanethiolate (SC_nH_{2n+1}=S*C*n) is, under electrochemical conditions, significantly affected by the penetration of solvents and electrolytes into the S*C*n layer. In this study, we estimated the charging energy $E_C(n)$ associated with $[PtAu_{24}(SCn)_{18}]^- + e^- \rightarrow [PtAu_{24}(SCn)_{18}]^{2-}$ (n=4, 8, 12, and 16) in vacuum using mass-selected gas-phase anion photoelectron spectroscopy of $[PtAu_{24}(SCn)_{18}]^z$ (z=−1 and −2). The $E_C(n)$ values of $PtAu_{24}(SCn)_{18}$ in vacuum are significantly larger than those in solution and decrease with n in contrast to the behavior reported for $Au_{25}(SCn)_{18}$ in solution. The effective relative permittivity (ε_m*) of the S*C*n layer in vacuum is estimated to be 2.3–2.0 based on the double-concentric-capacitor model. Much smaller ε_m* values in vacuum than those in solution are explained by the absence of solvent/electrolyte penetration into the monolayer. The gradual decrease of ε_m* with n is ascribed to the appearance of an exposed surface region due to the bundle formation of long alkyl chains.

Introduction

Since the pioneering works by Murray and Whetten,[1,2] monodispersed gold clusters protected by monolayers of alkanethiolate (SC_nH_{2n+1}=S*C*n) have been extensively studied as a benchmark for systematic understanding of the quantum confinement effect on electrochemical behavior.[3] Monolayer-protected Au_x clusters (MPCs) with $x>130$ exhibit metal-like quantized double layer charging behavior with approximately regularly spaced voltammetric peaks (the average separation of $\Delta V°$) due to consecutive single-electron charging steps.[1–5] The charging energy, $E_C(n)$, is dependent on n and is given by:

$$E_C(n) = e\ \Delta V° \tag{1}$$

where e is the elementary charge. $\Delta V°$ can be estimated by classical electrostatics of a concentric capacitor composed of a spherical metallic core with radius r surrounded by a uniform S*C*n monolayer with the relative permittivity ε_m and the thickness d,

$$\Delta V° = \frac{e}{4\pi\varepsilon_0\varepsilon_m}\frac{d}{(r+d)r} \tag{2}$$

where ε_0 represents permittivity of vacuum. The best fitting was achieved by assuming that the S*C*n layer has an ε_m value similar to that of self-assembled monolayers (SAMs) of S*C*n on a flat Au surface (ε_m~2.6).[6] The detailed ε_m value decreased somewhat with n due to lower density of the perimeter region of the monolayer. The capacitance, $C=e/\Delta V°$, was on the order of sub-attoFarad for S*C*n-protected Au clusters[7–9] and Au_{130}, Au_{133}, and Au_{144} protected by other thiolates.[10–12]

In contrast, charging of molecular, ultrasmall Au MPCs occurs via the addition of an electron into a quantized orbital (reduction).[1–3,13] For example, the $E_C(n)$ value for a representative series of $Au_{25}(SCn)_{18}$ clusters was obtained as follows using a voltammetric method.[14] $[Au_{25}(SCn)_{18}]^0$ consists of an icosahedral Au_{13} core capped with six units of $Au_2(SCn)_3$.[15] Within the framework of superatom concept,[16–18] $[Au_{25}(SCn)_{18}]^0$ accommodates seven valence electrons in 1S and triply-degenerated 1P superatomic orbitals to form an open electron configuration $(1S)^2(1P)^5$ (Scheme 1).[19–23] The $E_C(n)$ value was estimated using the

[*] Y. Tasaka, Dr. M. Suyama, Dr. S. Ito, Prof. Dr. K. Koyasu, Prof. Dr. T. Tsukuda
Department of Chemistry, Graduate School of Science, The University of Tokyo
7-3-1 Hongo, Bunkyo-ku. Tokyo 113-0033 (Japan)
E-mail: tsukuda@chem.s.u-tokyo.ac.jp
Prof. Dr. M. Kappes
Institute of Physical Chemistry II, Karlsruher Institute of Technology
Fritz-Haber-Weg 2, 76131 Karlsruhe (Germany)
E-mail: manfred.kappes@kit.edu
Prof. Dr. F. Maran
Department of Chemistry, University of Padova
via Marzolo 1, 35131 Padova (Italy)
E-mail: flavio.maran@unipd.it
Prof. Dr. F. Maran
Department of Chemistry, University of Connecticut
55 North Eagleville Road, Storrs, Connecticut 06269 (USA)

© 2024 The Authors. Angewandte Chemie International Edition published by Wiley-VCH GmbH. This is an open access article under the terms of the Creative Commons Attribution Non-Commercial NoDerivs License, which permits use and distribution in any medium, provided the original work is properly cited, the use is non-commercial and no modifications or adaptations are made.

© 2024 The Authors. Angewandte Chemie International Edition published by Wiley-VCH GmbH

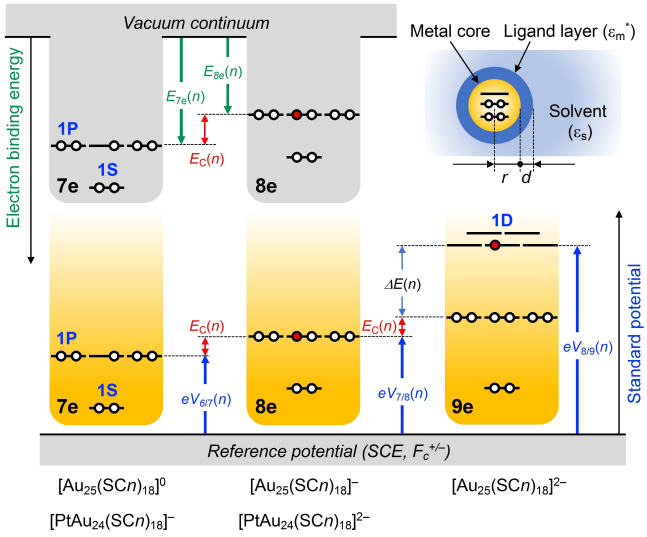

Scheme 1. Schematic energy level diagram of $[Au_{25}(SC\mathit{n})_{18}]^z$ and $[PtAu_{24}(SC\mathit{n})_{18}]^z$ for estimation of the charging energy $E_c(n)$ using voltammetry (bottom) and PES (top). For simplicity, this diagram ignores the energy splitting of 1P orbitals due to Jahn-Teller distortion of the $PtAu_{12}$ core and repulsive Coulomb barrier for $[PtAu_{24}(SC\mathit{n})_{18}]^{2-}$. The Au(5d) band located below the 1P orbitals is also omitted. *E*, Δ*E*, and *V* represent electron binding energy, energy gap between 1P and 1D orbitals, and redox potential, respectively. Inset shows a double concentric-capacitor model.

standard potentials of the 0/−1 and +1/0 redox couples ($V_{7/8}(n)$ and $V_{6/7}(n)$, respectively) by:[14]

$$E_C(n) = e\,\Delta V^\circ = e\,(V_{7/8}(n) - V_{6/7}(n)). \quad (3)$$

The $E_C(n)$ value given by eq. 3 is associated with the reduction $[Au_{25}(SC\mathit{n})_{18}]^0 + e \rightarrow [Au_{25}(SC\mathit{n})_{18}]^-$, which involves addition of an electron to the singly-occupied 1P orbital. Similarly, the energy required for $[Au_{25}(SC\mathit{n})_{18}]^- + e \rightarrow [Au_{25}(SC\mathit{n})_{18}]^{2-}$, which involves addition of an electron to the empty 1D orbital, can be estimated by $e\,(V_{8/9}(n) - V_{7/8}(n))$ where $V_{8/9}(n)$ and $V_{7/8}(n)$ are the standard potentials of the −1/−2 and 0/−1 redox couples, respectively (Scheme 1). However, this energy not only includes $E_C(n)$ obtained by eq. 3, but also the energy gap ($\Delta E(n)$) between 1P and 1D orbitals (Scheme 1), which can be calculated by (Table 1):

Table 1: Charging energies and HOMO–LUMO gaps of MPCs.[a]

Reactions	*n*	*d*/Å	E_C/eV	ε_m* [b]	ΔE[c]/eV	Ref.
$[Au_{25}(SC\mathit{n})_{18}]^0$ (7e)→	2	2.9	0.282	9.6	1.312	14
$[Au_{25}(SC\mathit{n})_{18}]^-$ (8e)	4	4.5	0.327	7.5	1.299	
	8	7.2	0.349	7.3	1.301	
	12	9.8	0.359	7.0	1.305	
	16	11.8	0.370	7.1	n.m.[d]	
$[PtAu_{24}(SC\mathit{n})_{18}]^-$ (7e)→	4	4.5	0.335	7.2		36
$[PtAu_{24}(SC\mathit{n})_{18}]^{2-}$ (8e)	6	6.1	0.34	7.1		37

[a] Measured in CH_2Cl_2 containing 0.1 M Bu_4NPF_6. [b] Calculated by using eq. 3, $r = 4.9$ Å, and $\varepsilon_s = 11$. [c] Determined for $[Au_{25}(SC\mathit{n})_{18}]^-$. [d] Not measurable.

$$\Delta E(n) = e\,(V_{8/9}(n) - V_{7/8}(n)) - E_C(n). \quad (4)$$

In conclusion, the $E_C(n)$ value corresponds to the energy required to put an electron into a singly-occupied orbital rather than into an empty orbital. Eqs. 3 and 4 have been conventionally used to estimate the charging energy and electrochemical energy gap between highest-occupied and lowest-unoccupied molecular orbitals (HOMO and LUMO) of various Au MPCs.[24]

Nevertheless, the $E_C(n)$ of $Au_{25}(SC\mathit{n})_{18}$ determined by eq. 3 could not be reproduced by eqs. 1 and 2 because the SC*n* ligands do not form a uniform SAM on the highly curved Au_{13} core. The short alkyl chains form a dynamic liquid-like shell, whereas the longer alkyl chains self-organize into bundles making the monolayer unevenly packed.[25] Consequently, the solvents and electrolytes partially penetrate the monolayer, leading to significant deviation of the effective permittivity of the SC*n* layer from that of the corresponding SAM on a flat Au surface. Because of these structural features, the permittivity of the SC*n* layer of $Au_{25}(SC\mathit{n})_{18}$ estimated using eq. 2 showed a counterintuitive trend to increase with increasing *n*.[14] To compensate for the breakdown of the concentric nanocapacitor model, Su et al. proposed a double-concentric-capacitor model in which the Au MPC is surrounded by solvent with a relative permittivity ε_s (Inset, Scheme 1):[26]

$$E_C(n) = e\Delta V^\circ = e\left[\frac{e}{4\pi\varepsilon_0\varepsilon_m^*}\frac{d}{(r+d)r} + \frac{e}{4\pi\varepsilon_0\varepsilon_s}\frac{1}{(r+d)}\right] \quad (5)$$

where ε_m* is effective relative permittivity of the SC*n* layer under the influence of the solvent and electrolyte. By fitting the $E_C(n)$ values of $Au_{25}(SC\mathit{n})_{18}$ using eq. 5, Antonello et al. successfully obtained a reasonable trend that the ε_m* values decrease monotonically with *n* and converge to a constant value of about 7 (Table 1).[14]

These analyses raise the simple question: how does the $E_C(n)$ value of $Au_{25}(SC\mathit{n})_{18}$ vary with *n* in the *absence of solvent or electrolyte*? A similar question was raised by Weaver and Gao, who suggested the concept of "molecular capacitance" by interrelating the charging energies of metal clusters in solution and in vacuum.[27] According to the generalized Koopmans' theorem,[28,29] the $E_C(n)$ value of $Au_{25}(SC\mathit{n})_{18}$ in vacuum ($\varepsilon_s = 1$) corresponds to the energy upshift of 1P orbitals upon electron attachment $[Au_{25}(SC\mathit{n})_{18}]^0 + e \rightarrow [Au_{25}(SC\mathit{n})_{18}]^-$ (Scheme 1), which can be estimated by:

$$E_C(n) = E_{7e}(n) - E_{8e}(n). \quad (6)$$

where $E_{7e}(n)$ and $E_{8e}(n)$ are the energy required for the detachment of an electron from $[Au_{25}(SC\mathit{n})_{18}]^0$ and $[Au_{25}(SC\mathit{n})_{18}]^-$ into vacuum, respectively. To determine $E_{7e}(n)$ and $E_{8e}(n)$ by photoelectron spectroscopy (PES) in gas phase,[30,31] we used mono-platinum doped analogues $PtAu_{24}(SC\mathit{n})_{18}$[32–35] instead of $Au_{25}(SC\mathit{n})_{18}$ because of the following reasons. (1) $[PtAu_{24}(SC\mathit{n})_{18}]^0$ has a similar geometric structure to that of $[Au_{25}(SC\mathit{n})_{18}]^-$: a slightly flattened

© 2024 The Authors. Angewandte Chemie International Edition published by Wiley-VCH GmbH

15213773, 2024, 37, Downloaded from https://onlinelibrary.wiley.com/doi/10.1002/anie.202408335 by Karlsruher Institut F., Wiley Online Library on [07/10/2024]. See the Terms and Conditions (https://onlinelibrary.wiley.com/terms-and-conditions) on Wiley Online Library for rules of use; OA articles are governed by the applicable Creative Commons License

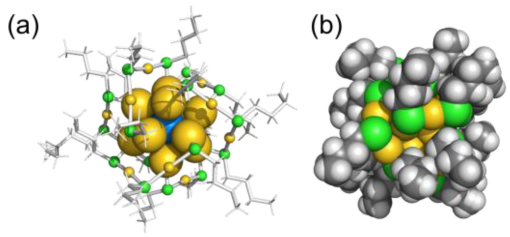

Figure 1. (a) Ball-and-stick and (b) space-filling representations of crystal structure of $[PtAu_{24}(SC_4H_9)_{18}]^0$.[37] Color codes: yellow, Au; blue, Pt; green, S.

icosahedral $Pt@Au_{12}$ core is protected by six units of $Au_2(SCn)_3$ (Figure 1).[32,36,37] (2) $[PtAu_{24}(SCn)_{18}]^-$ and $[PtAu_{24}(SCn)_{18}]^{2-}$ are isoelectronic to $[Au_{25}(SCn)_{18}]^0$ and $[Au_{25}(SCn)_{18}]^-$, respectively, and have negative charges for mass selection in vacuum. (3) The $E_C(n)$ values reported for $[PtAu_{24}(SCn)_{18}]^- + e \rightarrow [PtAu_{24}(SCn)_{18}]^{2-}$ in solution (Table 1) are similar to those for $[Au_{25}(SCn)_{18}]^0 + e \rightarrow [Au_{25}(SCn)_{18}]^-$.[36,37] In this work, we conducted PES on mass-selected beams of $[PtAu_{24}(SCn)_{18}]^-$ and $[PtAu_{24}(SCn)_{18}]^{2-}$ ($n=4$, 8, 12, and 16) to determine the $E_{7e}(n)$ and $E_{8e}(n)$ values, respectively. We found that the $E_C(n)$ values estimated by eq. 6 are significantly larger than those in solution (Table 1) and decrease with n in contrast to the behavior observed for $[Au_{25}(SCn)_{18}]^0$ in solution. Moreover, the ε_m* values in vacuum are estimated to be 2.3–2.0 using eq. 5, which are significantly smaller than those in solution (Table 1). This finding can be explained by the fact that the occupancy of vacuum in the monolayer increases with n.

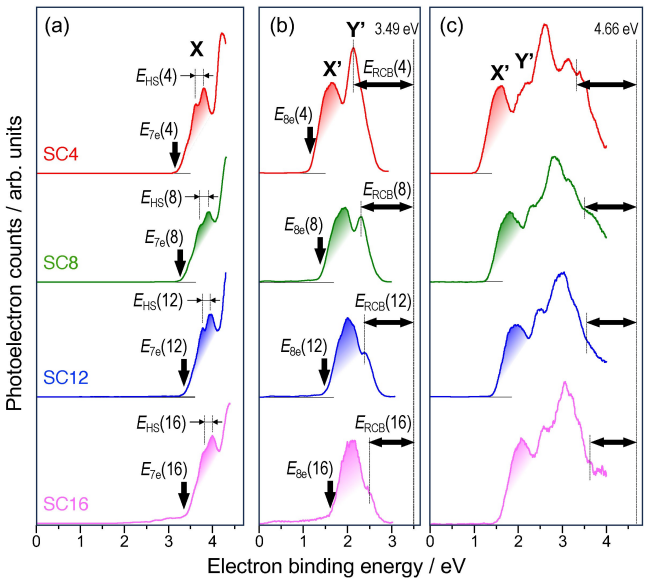

Figure 2. PE spectra of (a) $[PtAu_{24}(SCn)_{18}]^-$ recorded at 266 nm and $[PtAu_{24}(SCn)_{18}]^{2-}$ recorded at (b) 355 nm and (c) 266 nm. Downward arrows in panels (a) and (b) indicate the $E_{7e}(n)$ and $E_{8e}(n)$ values, respectively. Double arrows indicate $E_{RCB}(n)$ values of $[PtAu_{24}(SCn)_{18}]^{2-}$.

Table 2: Summary of PES results.

n	E_{7e}/eV	E_{HS}/eV	E_{8e}/eV	E_C/eV	E_{RCB}/eV
4	3.25	0.21	1.10	2.15	1.4
8	3.34	0.22	1.32	2.02	1.2
12	3.42	0.20	1.47	1.95	1.1
16	3.42	0.21	1.59	1.83	1.0

Results and Discussion

Gas-phase PES of chemically synthesized $[PtAu_{24}(SCn)_{18}]^-$ and $[PtAu_{24}(SCn)_{18}]^{2-}$ was conducted by using a home-built apparatus (Figure S1).[38] Details of the procedure are given in the Supporting Information. The PE spectra of $[PtAu_{24}(SCn)_{18}]^-$ and $[PtAu_{24}(SCn)_{18}]^{2-}$ recorded at 266 nm are presented in Figures 2a and 2c, respectively. The lowest energy bands for $[PtAu_{24}(SCn)_{18}]^-$ (band X in Figure 2a) and $[PtAu_{24}(SCn)_{18}]^{2-}$ (band X′ in Figure 2c) are assigned to the superatomic 1P orbitals, while band Y′ in $[PtAu_{24}(SCn)_{18}]^{2-}$ is assigned to Au(5d) bands based on the previous DFT study on the model structure $[PtAu_{24}(SH)_{18}]^{2-}$:[34] the orbitals below the 1P orbitals have large contribution from Au(5d). Band X in Figure 2a exhibits a small peak at lower E_B side. We call this energy gap $E_{HS}(n)$, whose values are listed in Table 2. Our DFT calculations illustrated that triply-degenerated 1P orbitals of $[PtAu_{24}(SC1)_{18}]^{2-}$ split into two subsets in $[PtAu_{24}(SC1)_{18}]^-$ with an energy difference of 0.12 eV (Figure S4). This splitting can be rationalized by Jahn–Teller distortion of the $PtAu_{12}$ core.[36] According to this calculation, the $E_{HS}(n)$ correspond to the energy difference between singly-occupied 1P orbital and HOMO-1 in $[PtAu_{24}(SCn)_{18}]^-$. Similarly, the HOMO–LUMO gap (E_{HL}) of $[PtAu_{24}(SCn)_{18}]^0$ can be approximated by $E_{HS}(n)$ of $[PtAu_{24}(SCn)_{18}]^-$ if we assume that the energy gap between the split 1P orbitals of $[PtAu_{24}(SCn)_{18}]^-$ is retained in $[PtAu_{24}(SCn)_{18}]^0$. Such assumption has been conventionally made for the estimation of E_{HL} of naked metal clusters with closed electronic shell based on the anion PES.[39–41] The $E_{HS}(n)$ values so estimated are comparable to those of $[PtAu_{24}(SCn)_{18}]^0$ in the liquid phase (0.38 eV for $n=4$,[36] 0.29 eV for $n=6$[37]) and show no dependence on the alkyl chain length. These results indicate that both HOMO and LUMO are stabilized in the solvated environment while keeping their relative energies constant.

The $E_{7e}(n)$ and $E_{8e}(n)$ values determined by the spectral onsets are indicated by downward arrows in Figure 2a and 2b, respectively, and are summarized in Table 2. Note that band X of $[PtAu_{24}(SC16)_{18}]^-$ shows a tailing structure in the smaller E_B range of 2.5–3.3 eV. This is due to the contamination of the $[PtAu_{24}(SC16)_{18}]^-$ beam with its dimer $[(PtAu_{24}(SC16)_{18})^-]_2$ having the same m/z value rather than two-photon electron detachment process via electronically-excited states as proven in Figure S5. Attempts to completely suppress the dimer formation by varying the sample concentrations were not successful due to strong vdW interactions between the long alkyl chains of $[PtAu_{24}(SC16)_{18}]^-$.[42] Both $E_{7e}(n)$ and $E_{8e}(n)$ increase with n (Table 2), indicating the longer alkyl chains stabilize the electrons more than the shorter alkyl chains. The energy

© 2024 The Authors. Angewandte Chemie International Edition published by Wiley-VCH GmbH

15213773, 2024, 37, Downloaded from https://onlinelibrary.wiley.com/doi/10.1002/anie.202408335 by Karlsruher Institut F., Wiley Online Library on [07/10/2024]. See the Terms and Conditions (https://onlinelibrary.wiley.com/terms-and-conditions) on Wiley Online Library for rules of use; OA articles are governed by the applicable Creative Commons License

shift of $E_{8e}(n)$ is larger than that of $E_{7e}(n)$. This result indicates the degree of stabilization is larger for $z=-2$ than for $z=-1$.

The $E_{7e}(n)$ is significantly larger than $E_{8e}(n)$ regardless of n due to electronic charging (Scheme 1). The $E_C(n)$ values of $PtAu_{24}(SCn)_{18}$ in vacuum were calculated using eq. 6 and are listed in Table 2 and plotted in Figure 3. The $E_C(n)$ values in Table 2 are (i) significantly larger than those of $Au_{25}(SCn)_{18}$ in solution (Table 1) and (ii) show opposite dependence with respect to n. This n-dependence of $E_C(n)$ can be qualitatively explained as follows using eq 5. The first and second terms in the bracket of eq. 5 correspond to the potential difference between Au core and outside of ligand layer and that between outside of the ligand layer and the infinity point in vacuum or solvent/electrolyte, respectively. When ε_s is relatively large ($\varepsilon_s=12.5$ in CH_2Cl_2 containing 0.1 M Bu_4NClO_4),[14] $E_C(n)$ is dominated by the first term, and thus increases with d (or n). On the other hand, when ε_s is small, as in vacuum ($\varepsilon_s=1$), the n dependence of $E_C(n)$ is governed by that of the second term and, therefore, $E_C(n)$ decreases with d (or n). To further rationalize the difference between the charging behavior of $PtAu_{24}(SCn)_{18}$ in solution and in vacuum, the ε_m* value of the ligand layer in vacuum was estimated by fitting the PES-determined $E_C(n)$ values using eq. 5. In the fitting, we fixed the ε_s and r values to 1 and 4.9 Å,[14] respectively, and the d values were those estimated from the diffusion coefficient of $[Au_{25}(SCn)_{18}]^0$ (see Table 3).[14] The $E_C(n)$ values were calculated by changing the ε_m* value by 0.1 increments, and then compared with the experimental $E_C(n)$ values. The charging energies $E_C^c(n)$ thus optimized are summarized in Table 3. The resulting ε_m* values decrease from 2.3 at $n=4$ to 2.0 at $n=16$ and are slightly smaller than the value estimated for the SAM of SCn on the extended Au surface (2.6).[6] This n-dependence for longer alkyl chains can be rationalized by bundle formation into opposite directions as previously observed in solution (Figure 3),[14] leaving the metal core around the "belt" region exposed to the external environment. Such bundle formation is expected to be even more pronounced in vacuum ($\varepsilon_s=1$), as can already be inferred from NMR measurements in benzene ($\varepsilon_s=2.27$).[14] Therefore, as n increases from 4 to 16, the contribution from the vacuum becomes even more important, thereby lowering the ε_m* further from the value expected for homogeneously distributed alkyl chains (2.6).[6] In other words, the ε_m* values in solution are larger than those in vacuum (Table 1) because the solvent and electrolyte with higher ε_s penetrate into the ligand layer, as already discussed.[14]

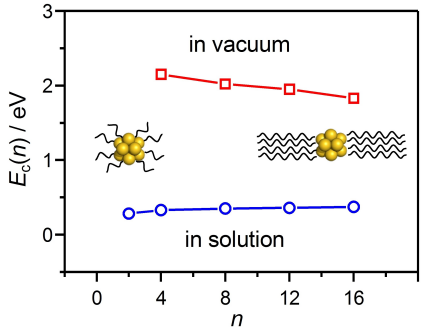

Figure 3. $E_C(n)$ of $Au_{25}(SCn)_{18}$ in solution (ref. [14]) and $PtAu_{24}(SCn)_{18}$ in vacuum (this work) as a function of n.

Table 3: Experimental and calculated charging energies.

n	r/Å[a]	d/Å[b]	ε_m*	E_C^c/eV[b]	E_C/eV[c]
4	4.9	4.5	2.3	2.14	2.15
8		7.2	2.1	2.02	2.02
12		9.8	2.0	1.96	1.95
16		11.8	2.0	1.90	1.83

[a] Ref. [43]. [b] calculated by eq. 2 with $\varepsilon_s=1$. [c] determined by PES.

Based on the structural insights into the monolayers, we discuss the effect of a ligand layer on the electron detachment process from doubly-charged anion $[PtAu_{24}(SCn)_{18}]^{2-}$. The PE spectra of $[PtAu_{24}(SCn)_{18}]^{2-}$ (Figures 2b and 2c) exhibited cut-off in high E_B region due to the repulsive Coulomb barrier (RCB)[44–46] between the detached electron and the remaining mono-anion $[PtAu_{24}(SCn)_{18}]^-$. The height of RCB (E_{RCB}) was experimentally estimated by the shape analysis of band Y′ in the PE spectra of $[PtAu_{24}(SCn)_{18}]^{2-}$ (Figure 2b). Band Y′ recorded at 355 nm (Figure 2b) looks thinner than that recorded at 266 nm (Figure 2c), because the high E_B side of band Y′ is cut off by the RCB. The E_{RCB} values were determined by subtracting the E_B value at the peak position of band Y′ (Figure 2b) from the photon energy (3.49 eV) and are listed in Table 2. Assuming that the E_{RCB} is determined purely by the electrostatic repulsion between the electron and $[PtAu_{24}(SCn)_{18}]^-$, the ΔV° term of eq. 5 corresponds to the potential rise when the electron reaches the core surface from the infinity point (Figure S6). Under this simple assumption, the E_{RCB} should agree with the E_C value given by eq. 5. However, the E_{RCB} values were significantly smaller than the E_C values by ~0.8 eV regardless of n (Table 2). This discrepancy suggests that the effective RCB height for electron detachment from $[PtAu_{24}(SCn)_{18}]^{2-}$ is lowered due to, for example, the attractive potential from the positive background of the $PtAu_{12}$ core. Table 2 shows that as n increases, the E_{RCB} value decreases as well as the E_C value. This trend suggests that both n-dependencies have similar origins. As discussed in the previous paragraph, the monolayer of long alkyl chains is not uniform in density due to the formation of bundles. The "local" permittivity in the bundles is expected to be larger than that in the naked belt region and close to the value of SCn SAM (2.6),[6] suggesting that the effective RCB height in the bundles is lower than that in the naked surface. We therefore propose that the RCB height is not uniform over the surface and that bundle of the long alkyl chains provides a lowest-energy route for electron detachment.

Conclusion

In summary, we conducted gas-phase anion photoelectron spectroscopy on $[PtAu_{24}(SCn)_{18}]^-$ and $[PtAu_{24}(SCn)_{18}]^{2-}$ ($n=$ 4, 8, 12, and 16) and estimated the charging energy $E_C(n)$

© 2024 The Authors. Angewandte Chemie International Edition published by Wiley-VCH GmbH

15213773, 2024, 37, Downloaded from https://onlinelibrary.wiley.com/doi/10.1002/anie.202408335 by Karlsruher Institut F., Wiley Online Library on [07/10/2024]. See the Terms and Conditions (https://onlinelibrary.wiley.com/terms-and-conditions) on Wiley Online Library for rules of use; OA articles are governed by the applicable Creative Commons License

associated with the redox process between the 7e and 8e superatomic states. We found that the $E_C(n)$ values in vacuum are significantly larger than those reported in solution[14] and decrease with n in contrast to the case for dissolved $Au_{25}(SCn)_{18}$. Compared to the species in solution, the PES data show that the charging behavior of $PtAu_{24}(SCn)_{18}$ in the isolated state is significantly contributed to by the vacuum's relative permittivity, i.e. the effective relative permittivity of the monolayer is lowered due to SCn bundling. This study not only proposes a new approach to evaluate the charging energy of MPCs using gas-phase photoelectron spectroscopy but also highlights significant effects of monolayer structures on charging behavior of MPCs.

Supporting Information

The authors have cited additional references within the Supporting Information.[47–53]

Acknowledgements

This research was supported financially by JST, CREST (Grant No. JPMJCR20B2).

Conflict of Interest

The authors declare no conflict of interest.

Data Availability Statement

The data that support the findings of this study are available from the corresponding author upon reasonable request.

Keywords: gold cluster compounds · charging energy · monolayer structure · photoelectron spectroscopy

[1] R. S. Ingram, M. J. Hostetler, R. W. Murray, T. G. Schaaff, J. T. Khoury, R. L. Whetten, T. P. Bigioni, D. K. Guthrie, P. N. First, *J. Am. Chem. Soc.* **1997**, *119*, 9279–9280.
[2] S. Chen, R. S. Ingram, M. J. Hostetler, J. J. Pietron, R. W. Murray, T. G. Schaaff, J. T. Khoury, M. M. Alvarez, R. L. Whetten, *Science* **1998**, *280*, 2098–2101.
[3] R. W. Murray, *Chem. Rev.* **2008**, *108*, 2688–2720.
[4] B. M. Quinn, P. Liljeroth, V. Ruiz, V. T. Laaksonen, K. Kontturi, *J. Am. Chem. Soc.* **2003**, *125*, 6644–6645.
[5] T. Dainese, S. Antonello, S. Bonacchi, D. Morales-Martinez, A. Venzo, D. M. Black, M. Mozammel Hoque, R. L. Whetten, F. Maran, *Nanoscale* **2021**,*13*, 15394–15402.
[6] M. D. Porter, T. B. Bright, D. L. Allara, C. E. D. Chidsey, *J. Am. Chem. Soc.* **1987**, *109*, 3559–3568.
[7] S. Chen, R. W. Murray, S. W. Feldberg, *J. Phys. Chem. B* **1998**, *102*, 9898–9907.
[8] R. Guo, D. Georganopoulou, S. W. Feldberg, R. L. Donkers, R. W. Murray, *Anal. Chem.* **2005**, *77*, 2662–2669.
[9] T. Laaksonen, O. Pelliniemi, B. M. Quinn, *J. Am. Chem. Soc.* **2006**, *128*, 14341–14346.
[10] A. H. Holm, M. Ceccato, R. L. Donkers, L. Fabris, G. Pace, F. Maran, *Langmuir* **2006**, *22*, 10584–10589.
[11] V. R. Jupally, J. G. Thrasher, A. Dass, *Analyst* **2014**, *139*, 1826–1829.
[12] S. Chen, T. Higaki, H. Ma, M. Zhu, R. Jin, G. Wang, *ACS Nano* **2020**, *14*, 16781–16790.
[13] S. Antonello, F. Maran, *Curr. Opin. Electrochem.* **2017**, *2*, 18–25.
[14] S. Antonello, T. Dainese, M. De Nardi, L. Perotti, F. Maran, *ChemElectroChem* **2016**, *3*, 1237–1244.
[15] T. Dainese, S. Antonello, J. A. Gascûn, F. Pan, N. V. Perera, M. Ruzzi, A. Venzo, A. Zoleo, K. Rissanen, F. Maran, *ACS Nano* **2014**, *8*, 3904–3912.
[16] S. Khanna, P. Jena, *Phys. Rev. Lett.* **1992**, *69*, 1664–1667.
[17] J. U. Reveles, S. N. Khanna, P. J. Roach, A. W. Castleman, *Proc. Natl. Acad. Sci. USA* **2006**, *103*, 18405–18410.
[18] H. Häkkinen, *Chem. Soc. Rev.* **2008**, *37*, 1847–1859.
[19] J. Akola, M. Walter, R. L. Whetten, H. Häkkinen, H. Grönbeck, *J. Am. Chem. Soc.* **2008**, *130*, 3756–3757.
[20] M. Walter, J. Akola, O. Lopez-Acevedo, P. D. Jadzinsky, G. Calero, C. J. Ackerson, R. L. Whetten, H. Grönbeck, H. Häkkinen, *Proc. Natl. Acad. Sci. USA* **2008**, *105*, 9157–9162.
[21] M. Zhu, C. M. Aikens, F. J. Hollander, G. C. Schatz, R. Jin, *J. Am. Chem. Soc.* **2008**, *130*, 5883–5885.
[22] A. Munoz-Castro, *Phys. Chem. Chem. Phys.* **2019**, *21*, 13022–13029.
[23] Q. Tang, F. Li, D.-e. Jiang, *ACS Nanosci. Au* **2022**, *2*, 40–48.
[24] K. Kwak, D. Lee, *Acc. Chem. Res.* **2019**, *52*, 12–22.
[25] S. Antonello, G. Arrigoni, T. Dainese, M. De Nardi, G. Parisio, L. Perotti, A. René, A. Venzo, F. Maran, *ACS Nano* **2014**, *8*, 2788–2795.
[26] B. Su, M. Zhang, Y. Shao, H. H. Girault, *J. Phys. Chem. B* **2006**, *110*, 21460–21466.
[27] M. J. Weaver, X. Gao, *J. Phys. Chem.* **1993**, *97*, 332–338.
[28] J. Akola, M. Manninen, H. Häkkinen, U. Landman, X. Li, L.-S. Wang, *Phys. Rev. B* **1999**, *60*, R11297–R11300.
[29] H. Häkkinen, B. Yoon, U. Landman, X. Li, H. J. Zhai, L.-S. Wang, *J. Phys. Chem. A* **2003**, *107*, 6168–6175.
[30] K. Hirata, R. Tomihara, K. Kim, K. Koyasu, T. Tsukuda, *Phys. Chem. Chem. Phys.* **2019**, *21*, 17463–17474.
[31] K. Koyasu, T. Tsukuda, *J. Chem. Phys.* **2021**, *154*, 140901.
[32] H. Qian, D.-e. Jiang, G. Li, C. Gayathri, A. Das, R. R. Gil, R. Jin, *J. Am. Chem. Soc.* **2012**, *134*, 16159–16162.
[33] K. Kwak, W. Choi, Q. Tang, M. Kim, Y. Lee, D.-e. Jiang, D. Lee, *Nat. Commun.* **2017**, *8*, 14723.
[34] F. Alkan, P. Pandeya, C. M. Aikens, *J. Phys. Chem. C* **2019**, *123*, 9516–9527.
[35] W. Choi, H. Seong, V. Efremov, Y. Lee, S. Im, D.-H. Lim, J. S. Yoo, D. Lee, *J. Chem. Phys.* **2021**, *155*, 014305.
[36] W. Fei, S. Antonello, T. Dainese, A. Dolmella, M. Lahtinen, K. Rissanen, A. Venzo, F. Maran, *J. Am. Chem. Soc.* **2019**, *141*, 16033–16045.
[37] K. Kwak, Q. Tang, M. Kim, D.-e. Jiang, D. Lee, *J. Am. Chem. Soc.* **2015**, *137*, 10833–10840.
[38] S. Ito, Y. Tasaka, K. Nakamura, Y. Fujiwara, K. Hirata, K. Koyasu, T. Tsukuda, *J. Phys. Chem. Lett.* **2022**, *13*, 5049–5055.
[39] R. Busani, M. Folkers, O. Cheshnovsky, *Phys. Rev. Lett.* **1998**, *81*, 3836–3839.
[40] J. Li, X. Li, H.-J. Zhai, L.-S. Wang, *Science* **2003**, *299*, 864–867.
[41] A. Lechtken, D. Schooss, D. J. R. Stairs, M. N. Blom, F. Furche, N. Morgner, O. Kostko, B. von Issendorff, M. M. Kappes, *Angew. Chem. Int. Ed.* **2007**, *46*, 2944–2948.
[42] M. Suyama, S. Takano, T. Tsukuda, *J. Am. Chem. Soc.* **2023**, *145*, 3361–3368.

© 2024 The Authors. Angewandte Chemie International Edition published by Wiley-VCH GmbH

15213773, 2024, 37, Downloaded from https://onlinelibrary.wiley.com/doi/10.1002/anie.202408335 by Karlsruher Institut F., Wiley Online Library on [07/10/2024]. See the Terms and Conditions (https://onlinelibrary.wiley.com/terms-and-conditions) on Wiley Online Library for rules of use; OA articles are governed by the applicable Creative Commons License

[43] T. Dainese, S. Antonello, J. A. Gascón, F. Pan, N. V. Perera, M. Ruzzi, A. Venzo, A. Zoleo, K. Rissanen, F. Maran, *ACS Nano* **2014**, *8*, 3904–3912.
[44] L.-S. Wang, X.-B. Wang, *J. Phys. Chem. A* **2000**, *104*, 1978–1990.
[45] P. D. Dau, H.-T. Liu, J.-P. Yang, M.-O. Winghart, T. J. A. Wolf, A.-N. Unterreiner, P. Weis, Y.-R. Miao, C.-G. Ning, M. M. Kappes, L.-S. Wang, *Phys. Rev. A* **2012**, *85*, 064503.
[46] A. P. Veenstra, L. Monzel, A. Baksi, J. Czekner, S. Lebedkin, E. K. Schneider, T. Pradeep, A.-N. Unterreiner, M. M. Kappes, *J. Phys. Chem. Lett.* **2020**, *11*, 2675–2681.
[47] E. Ito, S. Ito, S. Takano, T. Nakamura, T. Tsukuda, *JACS Au* **2022**, *2*, 2627–2634.
[48] K. Nakamura, S. Ito, K. Koyasu, T. Tsukuda, *Phys. Chem. Chem. Phys.* **2023**, *25*, 5955–5959.
[49] S. Takano, S. Ito, T. Tsukuda, *J. Am. Chem. Soc.* **2019**, *141*, 15994–16002.
[50] B. J. Gregory, C. K. Ingold, *J. Chem. Soc. B* **1969**, 276–289.
[51] M. Suyama, S. Takano, T. Nakamura, T. Tsukuda, *J. Am. Chem. Soc.* **2019**, *141*, 14048–14051.
[52] M. J. Frisch, G. W. Trucks, H. B. Schlegel, G. E. Scuseria, M. A. Robb, J. R. Cheeseman, G. Scalmani, V. Barone, G. A. Petersson, H. Nakatsuji, X. Li, M. Caricato, A. V. Marenich, J. Bloino, B. G. Janesko, R. Gomperts, B. Mennucci, H. P. Hratchian, J. V. Ortiz, A. F. Izmaylov, J. L. Sonnenberg, D. Williams-Young, F. Ding, F. Lipparini, F. Egidi, J. Goings, B. Peng, A. Petrone, T. Henderson, D. Ranasinghe, V. G. Zakrzewski, J. Gao, N. Rega, G. Zheng, W. Liang, M. Hada, M. Ehara, K. Toyota, R. Fukuda, J. Hasegawa, M. Ishida, T. Nakajima, Y. Honda, O. Kitao, H. Nakai, T. Vreven, K. Throssell, J. A. Montgomery Jr., J. E. Peralta, F. Ogliaro, M. J. Bearpark, J. J. Heyd, E. N. Brothers, K. N. Kudin, V. N. Staroverov, T. A. Keith, R. Kobayashi, J. Normand, K. Raghavachari, A. P. Rendell, J. C. Burant, S. S. Iyengar, J. Tomasi, M. Cossi, J. M. Millam, M. Klene, C. Adamo, R. Cammi, J. W. Ochterski, R. L. Martin, K. Morokuma, O. Farkas, J. B. Foresman, D. J. Fox, *Gaussian 16, Revision B.01*, Gaussian, Inc., Wallingford CT **2016**.
[53] The PyMOL Molecular Graphics System, Version 2.6 Schrödinger, LLC.

Manuscript received: May 1, 2024
Accepted manuscript online: June 17, 2024
Version of record online: August 8, 2024

© 2024 The Authors. Angewandte Chemie International Edition published by Wiley-VCH GmbH

15213773, 2024, 37, Downloaded from https://onlinelibrary.wiley.com/doi/10.1002/anie.202408335 by Karlsruher Institut F., Wiley Online Library on [07/10/2024]. See the Terms and Conditions (https://onlinelibrary.wiley.com/terms-and-conditions) on Wiley Online Library for rules of use; OA articles are governed by the applicable Creative Commons License